Chapter 1

Thermal-Assisted Machining of Nickel-based Alloy

Erween Rahim, Norazlan Warap and Zazuli Mohid

Additional information is available at the end of the chapter

http://dx.doi.org/10.5772/61101

Abstract

Nickel-based alloy can be found in different industrial applications especially in aircraft engines and hot end components of various types of gas turbines with its high strength, strong corrosion resistance and excellent thermal fatigue properties and thermal stability compared to conventional materials. However, nickel-based alloy is one of the extremely difficult-to-cut materials. During the machining process, the interaction between the tool and the workpiece causes severe plastic deformation and intense friction at the tool-workpiece interface. Because of the increasing demands in industries, any improvement of conventional machining processes or any other deployment of additional technique is directly related to higher productivity. Thermal-assisted machining (TAM) has become an effective alternative to the conventional machining of these difficult-to-cut materials. Various types of heating methods and the beneficial effects on machining of nickel-based alloys are discussed in this chapter. Finally, TAM was proven as an efficient technique to increase the machinability of nickel-based alloys in terms of tool life, surface roughness and cutting force.

Keywords: thermal assisted machining, Hot machining, Nickel-based alloy

1. Introduction

The machinability index of work materials in machining are assessed in term of various aspects and criteria. Currently, the evaluation index includes tool life, cutting force, power requirements and surface finish. However, in this decade, sustainable machining is the most important criteria that need to be considered with the development of new techniques and methods for

machining. The machining technique can be assumed to be sustainable when it proves beneficial to the economy, environment and society. Machinability index of nickel-based alloy compared to carbon steel is 35 to 100 [1]. This means that machining of nickel-based alloy is more difficult than free-machining of carbon steel. The machining difficulties of nickel-based alloys originate from its excellent material properties with higher ductility and material strength at elevated temperatures. These will cause significant increments on the cutting temperature and decrements on tool life during the cutting process. Table 1 shows a summary of previous researches for various preheating methods.

Process	Preheating Methods	Workpiece/ Cutting Tool	Findings
Turning [2]	Laser	Inconel 718/carbide	With increased preheating temperatures to 620°C came a 25% decrease in specific cutting energy, an increase of 200%–300% tool life and improved surface roughness
Turning [3]	Plasma	Inconel 718/carbide	Improved surface roughness by 250%, decreased cutting force of around 30%–50% and extended tool life of up to 170% over conventional machining
Turning [4]	Laser	Inconel 718/carbide	In comparison with conventional cutting, the resultant force in LAM condition decreased by 24%–46%. However, the chip thickness increased 40% under LAM conditions by applying preheating temperatures of 800°C
Turning [5]	Oxyacetylene gas flame	Stainless steel/carbide	With preheating temperatures of 400°C, the material removal rate was maximized. Otherwise, cutting speed (31 m/min) was the most significant effect to minimize the surface roughness
Turning [6]	Electricity resistance	Ti-15333 alloy/carbide	It shows the significant reduction of cutting force in the range of 80%–85% when the preheating temperature applied was approximately 300°C
Turning [7]	Laser	42CrMo4 steel/carbide	The material strength was reduced when the preheating temperature was increased to 700°C. It was proved that the cutting force could decrease by as much as 40%
Milling [8]	Coil	AISI D2/cubic boron nitrate PCBN	By applying preheating temperatures of approximately 50°C–150°C, the surface roughness and charter result decreased compared to machining at room temperature
Turning [9]	Laser	Inconel 718/coated carbide and SiAlON ceramic	The surface finish improved by more than 25%, and the material removal rate increased by approximately 800%

Table 1. Summary of Preheating Methods

Generally, either conventional or advanced machining techniques have their own advantages and disadvantages. It must be chosen correctly based on the purpose and type of processes to be prepared. Selecting the right process can be maximizing production capacity and quality. Hybrid machining is another technique to enhance the machining performance and capability to cut material while minimizing the negative effects on the products and tools. Well-selected processing parameters and the combination between conventional and advanced machining techniques can efficiently increase the machining performance. A machining technique with the assistance of heat induction on nickel-based alloy was developed to counter this issue. Various heat sources such as laser, plasma, induction coil and flame heating were successfully applied in the machining process. The influence of heat on the materials' characteristics is one of the issues addressed in determining the heating and machining parameters. Categorized as nonferrous metals, nickel-based alloys show similar machining characteristics as other materials such as titanium and stainless steel. The equipment and methods used for heating gives significant influence to machinability.

The purpose of thermal-assisted machining processes is to reduce the cutting forces, prolong tool life, reduce chatter and improve surface finish. The reduction of total cutting length is associated with low shear yield strength of the work material at the primary and secondary shear planes. During the thermally assisted machining process, the plasticity of the work material increases, leading to the increment of chip-tool contact length, which plays an important role in reducing the normal stress acting on the tool [10]. Heating also reduces the intensity of chip serration, facilitating lower fluctuations of the cutting forces, which consequently reduce the dynamic stresses applied to the tool, thereby facilitating lower tool wear in heat-assisted machining.

2. Nickel-based alloy properties and its constraints

Nickel-based alloys are an important material in various industries, especially those involving high-temperature applications. They are widely used in gas turbine engines, aircrafts, nuclear reactors, submarines, steam power plants, petrochemical equipment and other higher-temperature applications. The excellent properties of nickel-based alloys at elevated temperature contribute to poor machinability and can be summarized as [11] (i) a major part of their strength is maintained during machining with higher ductility and yield strength; (ii) during the cutting process, work hardening rapidly occurs and contributes to tool wear and reduction of tool life; (iii) cutting tools suffer from high abrasive wear owing to the presence of hard abrasive carbides in the super alloy; (iv) chemical reactions occur at high cutting temperatures and leads to high diffusion wear rates; (v) adhesion of microchips onto the cutting tool frequently occurs during the cutting process and causes severe notching as well as spalling on the rack face and consequent pull-out of the coating materials; (vi) difficulties in controlling the formation of tough and continuous chips during the cutting process contributing to the degradation of the cutting tool performance; (vii) low thermal conductivity and poor thermal diffusivity of nickel-based alloys generate high temperatures on the tool tip and consequently increases the cutting temperature.

The alloying elements contained in the materials possess high strength and toughness over a wide temperature range and excellent fatigue strength, oxidation and corrosion resistance. However, the alloy was designed originally as a solid solution alloy and it has been shown that the precipitation of intermetallic phases occurs during the preheating process. For nickel-based alloys, strength is influenced by body-centred tetragonal (BCT) γ″ - Ni_3Nb and face-cantered cubic (FCC) γ′- Ni_3(Al,Ti) precipitates. This metastable phase precipitates on preheating temperature above 873 K [12]. The equilibrium intermetallic phase forms in alloy element when the formation of orthorhombic δ or Ni_3(Nb, Mo) phase occurs entirely and the stability of this phase will be sustained at elevated temperatures.

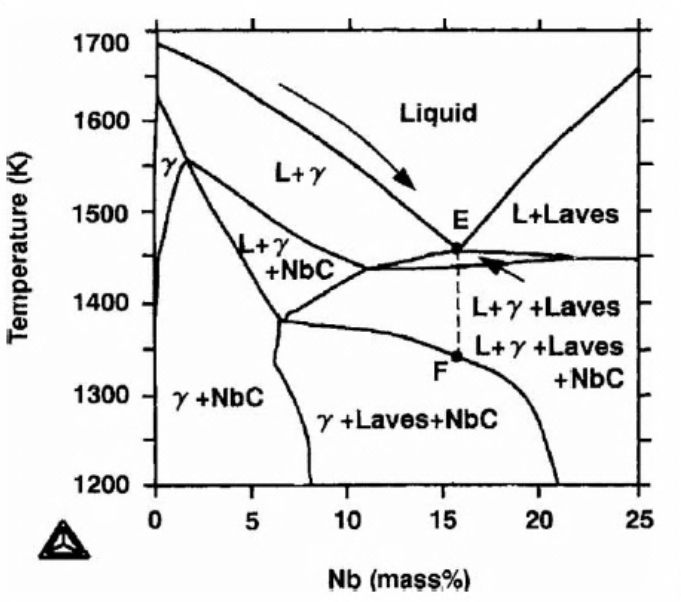

Figure 1. Phase diagram of Inconel 718 alloy calculated on the basis of Thermo-Calc software [12].

Moreover, Luo et al. [13] calculated a phase diagram for a nickel-based alloy database with Thermo-Calc, a multielement thermodynamic calculation software package and the results obtained are shown in Figure 1. According to this phase diagram, with a niobium concentration (5%), liquid phase is formed by a reaction between g and NbC in the temperature range of approximately 1420–1510 K and above, the NbC entirely disappears and leaves coexistent γ phase and liquid phase. The temperature at the liquid phase formed at 1440 K and the temperature at massive niobium carbides at 1530 K dissolved and disappeared. Both phases at different temperatures can be predicted from the phase diagram in Figure 1. Furthermore, the γ phase eutectic reaction occurs at a niobium concentration in the range of 11%–22%. At this phase, it means that the specimen has no change in the nature and initial properties and

http://dx.doi.org/10.5772/61101

the phase diagram seems to suggest that the niobium in the liquated microstructure is far more concentrated than in the solid γ phase.

In thermal-assisted machining, it can be assumed that it is effective when the preheating temperature is controlled under deformation temperature or in metastable phase. Each category of nickel-based alloys has different deformation temperatures where it is based on the alloy element contained in the materials' composition. Deformation temperature, strain rate and the deformation heat treatment are the main factors in determining which structural mechanism would control the flow stress value. Otherwise, utilization of proper temperature will affect the microstructure deformation in determining whether it is impressed with the effect of softening or hardening. However, deformation temperature and strain rate are the main variables in controlling the structural softening processes during hot deformation of the material.

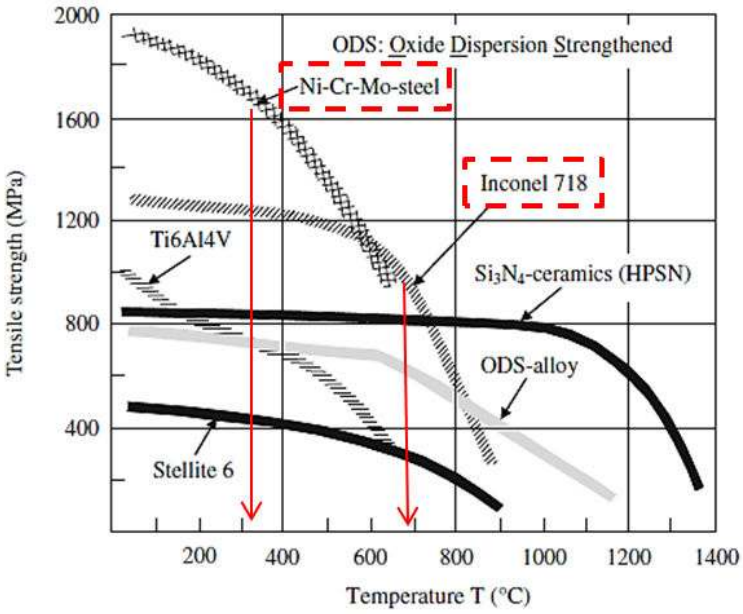

Figure 2. Effect of preheating temperature on the ultimate tensile strength for various materials [14].

Figure 2 shows the effect of preheating temperature on the ultimate tensile strength of various types of materials. In the category of nickel-based alloys, Ni-Cr-Mo steel exceeded the maximum ultimate yield strength at lower preheating temperatures of around 250°C–350°C. However, Inconel 718 with alloying elements of more than 50% have durable tensile strengths at elevated temperatures of around 600°C–700°C. In addition, the high temperature oxidation resistance has become more important, due to the fact that the demand for the development of higher temperature and more reliable Inconel 718 components in modern industry is

increasing. Currently, it is well recognized that poor oxidation resistance of any thermoresistance component can pose a potential risk to its service reliability leading to severe degradation of service life.

3. Temperature prediction

Prediction of heat generation and distribution initiated by laser irradiation using finite element analysis (FEA) software has been widely reported by many researchers. Saodari and Majumdar [15] used FEA to analyse the heating rate, heat-affected zone and the shape and size of the molten pool using a Gaussian laser beam. In addition, they also analysed the effect of mesh size to obtain accurate prediction results. Furthermore, Ren et al. [16] used FEA to analyse the effect of heat generated on residual stress during laser processing.

Further investigations have been done to find more accurate data about temperature distribution. Mohid et al. [17] reported the effect of absorptivity, A, and Gaussian distribution constant, K values, on the accuracy of the numerical analysis results. The investigation shows that the A and K values have a significant effect on the characterization of melting pool and heat-affected zone (HAZ) pattern. The calculation of the moving heat flux, the position and the magnitude of the heat flux were confirmed every time for pulsed laser heating. The distribution of heat flux is dependent on the pulsed length time. The Gaussian distribution theory on laser energy was used as a heat source on the upper surface. It can be expressed as shown in Equation 1.

$$q(x,y) = \frac{AKP}{S}\exp\left[\frac{-K(x^2+y^2)}{b^2}\right] \tag{1}$$

where x and y is the location from the laser beam centre, and b is the efficient beam radius. The laser power used is assumed as P. The absorptivity A is determined based on the type of material and surface roughness. However, the value of constant K depends on the beam's intensity. Several assumptions need to be considered to facilitate the simulation work. The assumption consists of (i) the material is homogenous, (ii) simulation is work on transient mode and (iii) the keyhole formation can be neglected.

Figure 3(a) and (b) show the thermal conductivity and specific heat, respectively, of Inconel 718 measured by various investigators. The spread in the data is relatively small, indicating that all of the data is precise and most likely accurate. Figure 3(c) shows the experimental value of spectral absorptivity for Inconel 718 [18]. The laser beam energy absorptivity of Inconel 718 is very low for CO_2 lasers, while it is higher for shorter wavelength lasers, such as Nd:YAG and diode lasers. The error of HAZ depth increases when the K value is 3. This is due to the laser intensity on Gaussian distribution in simulation, which was determined by the total energy density. The greater value of K produced higher laser beam density and this does not coincide with the actual situation during irradiation.

http://dx.doi.org/10.5772/61101

In FEA, the model can be assumed precise when the depth and width of the HAZ in the numerical simulation are comparable with the actual experiment. In this case, an error of less than 10% in the HAZ geometry compared to substantial geometry is acceptable to validate the model. The recorded HAZ temperature in the simulation reached 850 K. This represents the borderline of the HAZ area. The actual specimens that were exposed to the laser irradiation were cut perpendicular to the scanning direction at a distance of 15 to 20 mm from the starting point. Basically, the location is selected based on the stability of the heat generated and by heat absorption into the materials during the irradiation process.

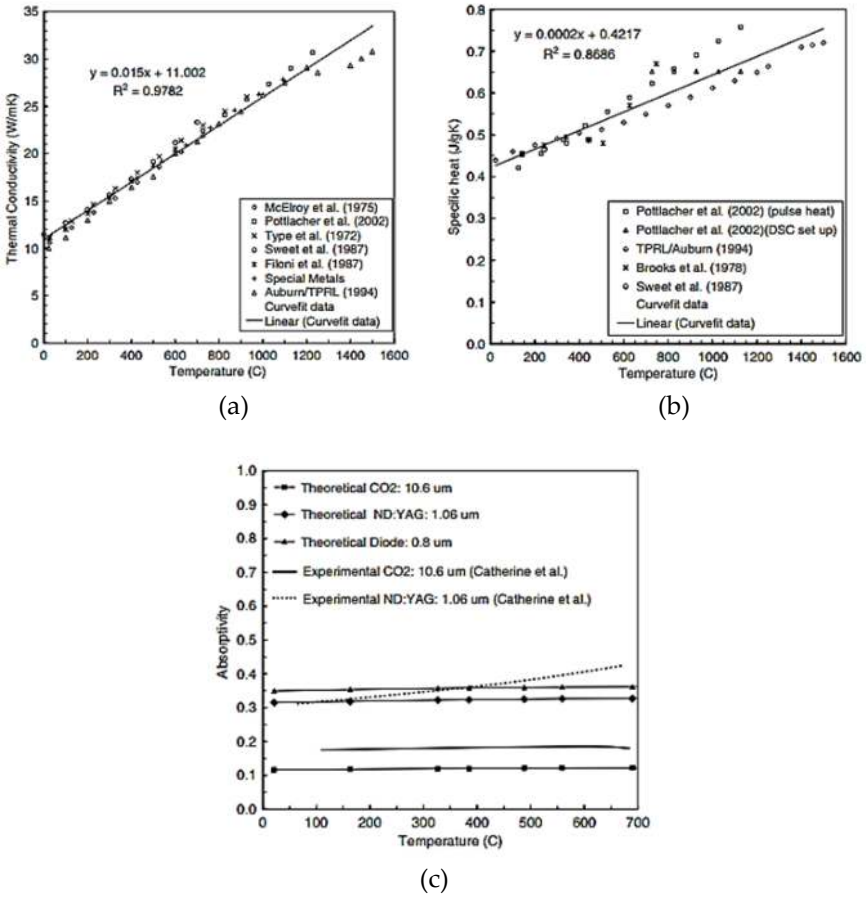

Figure 3. Comparison of temperature dependence state by various researchers on (a) thermal conductivity (b) specific heat and (c) theoretical and experimental normal spectral absorptivity at different laser wavelength of Inconel 718 [2].

Figure 4(a) and (b) show the results of experimental and simulation data for HAZ depth and width under a constant laser average power, P_{avg} 5.65 W and different absorptivity, A and K

values. It was noted that the error of melting width becomes smaller when a *K* value of 2.5 is applied. However, absorptivity also gives a significant effect on the formation of HAZ. Higher absorptivity is produced by the black surface. In the machining process, the workpiece is normally well prepared with good surface condition and dimension. Shining workpiece surface condition will reduce the absorptivity. Figure 4(b) shows the effect of absorptivity in simulation results. By increasing the *A* value from 30% to 40%, the error is higher than 5%. However, when the value of *A* is fixed at 35%, the error decreases to less than 5%. Furthermore, laser power also plays a significant role in the formation of the HAZ and melting region. As the laser power increases, the HAZ and melting region were formed a few microns underneath the surface. Finally, when the values of *A* and *K* were fixed to 35% and 2.5%, respectively, the result of HAZ width and depth are comparable with a percentage error of less than 10% as shown in Figure 4(c). A comparison image between simulation and actual specimenis shown in Figure 5.

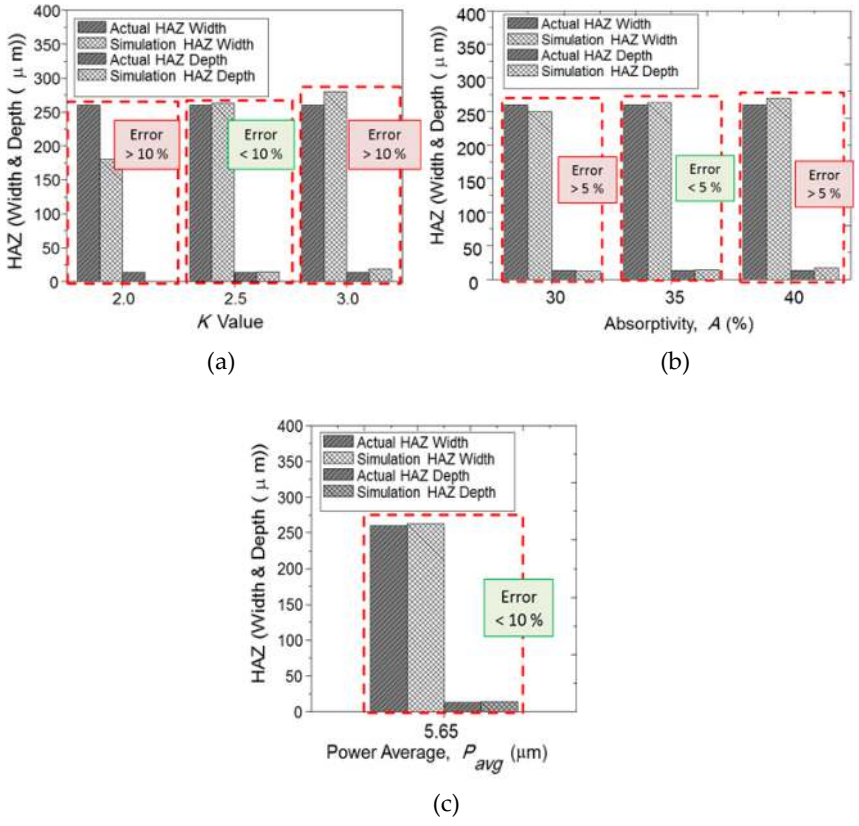

Figure 4. Effect of (a) *K* value (b) absorptivity, *A* in the formation of HAZ pattern and (c) model validation when the result of HAZ shape between actual scanning is comparable with simulation.

http://dx.doi.org/10.5772/61101

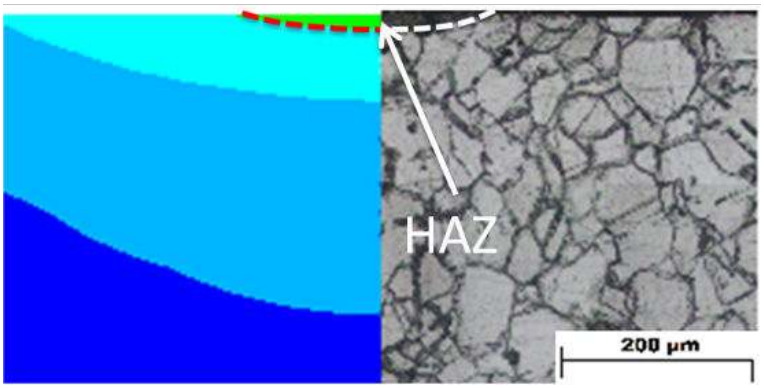

Figure 5. Comparison of HAZ shape size (P_{avg} = 5.65 W, A = 35% and K = 2.5) [19].

4. Heating methods in thermal-assisted machining

Thermal-assisted machining was introduced to overcome the machining issues regarding tool life, surface integrity and workpiece mechanical property changes. Theoretically, metal's strength and hardness decreases with increasing temperature. Heating metal below the deformation temperature will soften and reduce hardness and strength without major changes in its properties after it is chilled to room temperature. The same theory can be applied to all hot-machining processes such as hot forging, hot bending and hot stamping.

The methods of inducing heat energy into the workpiece gives different characteristics on the temperature distribution. Heat induction using a heating coil was reportedly applicable in machining [8, 20]. Oxyacetylene flame is one of the methods of applying heat to a workpiece. In micromachining, a concentrated and small heat source such as plasma and laser are preferable. In recent years, plasma and lasers have been reported to be the most promising heating techniques in thermal-assisted machining. Using laser or plasma beam is better in terms of heat distribution control. The focused and restricted heating area and easy-to-control scanning parameters will minimize thermal effects on workpieces. In thermal-assisted lathe machining, the type of heat source does not give a significant effect on machining performance compared to thermal-assisted milling. In the case of lathe machining, the heating area rotates at high speed and is repetitively heated as the specific point rotation through the laser or plasma beam focused area. The temperature gradually increases and fewer variations of gradual temperature can be seen along the cutting path. On the other hand, in thermally assisted milling processes, the heat source moves along with the tool and the heating efficiency is highly influenced by the scanning parameters, laser beam spot-to-cutting tool distance and spot size. The cutting area will be heated once and heat conduction and convection gives a significant effect on the temperature distribution characteristics.

Using a laser beam as the heat source exhibits significant effect on the temperature distribution characteristics. In general, continuous wave beam with a Gaussian distribution is preferable for the heating process. The workpiece can be heated up gradually with fewer thermal shock effects. When pulsed wave mode laser is used, heating and chilling will occur repeatedly on the workpiece. These phenomena will cause the material to undergo a hardening process and bring adverse effects on the machining performance. Thus, it is important to understand the method of preheating and its influences.

Various heat sources have been investigated as preheating media such as CO_2, Nd:YAG, diode laser and excimer laser. CO_2 laser has a wavelength of 10.6 μm and is ideal for optimum absorption, especially on ceramics, which is widely used. However, it has limitations where it requires a beam transfer method using a mirror as well as lower flexibility compared to a solid laser using fiber optic cables such as Nd:YAG laser. Table 2 summarizes the various types of preheat and heat sources with its different advantages and disadvantages. However, to have a user-friendly machine where the heat concentration is a priority, Nd:YAG laser is recommended compared to other laser sources.

Heat source	Advantages	Disadvantages
Laser	• High degree of heat concentration • Easy control of heat source	• Costly equipment • Absorption rate on different materials
Induction coil	• Easy to use • High-capacity preheating	• Impossible on high-concentration preheating • Limited tool mobility
Gas flame	• Low initial investment cost	• Impossible on high-concentration preheating
Plasma	• High degree of heat concentration	• Impossible to precisely control
Electricity	• Simple equipment • Even heat distribution	• Impossible to precisely control

Table 2. Heat Source/Heating Method Used

5. Plasma Enhancement Machining (PEM)

The ability to control the workpiece material at a constant degree of localized heating in the allocated cutting zone is the main critical issue contributing to the success of PEM. Direct current (d_c) is used to provide arcs resulting from reaction between electrode sparking and plasma gas to generate thermal or equilibrium plasma. Thoriated tungsten cathode and cooled nozzles are the main components producing plasma arc as shown in Figure 6. The nozzle can be assumed as a positive polarity (anode) when the workpiece material is nonconducting. Whereas, when the workpiece material is conductive, the nozzle can be assumed to have a negative polarity (cathode). Compared with a welding setup, there is a similarity in terms of

http://dx.doi.org/10.5772/61101

concept and operating mechanism. In case of machining of super alloy materials, high localized energy at low gas flow rate is suited to transfer arcs with typical peak temperatures of approximately 16,000 K.

Leshock et al. [21] performed an experiment to evaluate PEM system performance on turning operation. The main components of the experimental setup consisted of 7 HP lathes, a plasma heating system and control unit. A special enclosure was designed and attached to a turning chuck to minimize and prevent turbulent airflow generated by its rotation. Resulting from the previous study, the turbulent airflow could affect the concentration of plasma arc irradiation when cutting is near the chuck. Inconsistent results are produced from the turbulent airflow interference. To counter this issue, a copper nozzle was fitted with a 3.18 mm diameter orifice. Thoriated tungsten cathodes with a 20° included angle were used throughout the experiment. Various measurement methods and temperature values were used in the actual process and offline to evaluate the performance of hot turning. Finally, PEM significantly reduced the cutting forces and improved surface roughness over a wide range of cutting conditions.

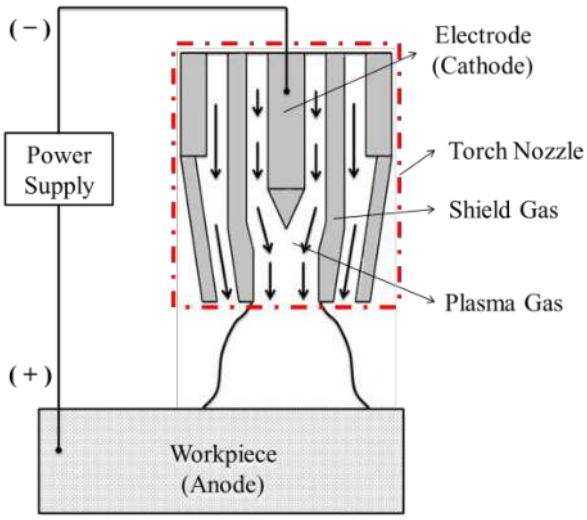

Figure 6. Plasma arc (transferred arc) generator.

Madhavulu and Ahmed [21] observed in their work that the major advantages of the plasma-assisted turning process are the increased metal removal rates, the lower spindle power requirement and the possibility of machining hard and tough metals even when fully hardened and heat-treated. The authors revealed that PEM leads to a 1.8 times gain in metal removal rate and 1.67 times prolonged tool life. However, the energy consumption used in the PEM system is far larger than the energy required for a machining process in conventional systems.

In addition, Leshock et al. [21] conducted a numerical and experimental study on PEM of Inconel 718. The surface temperature generated by the plasma system was measured by using

an infrared radiation thermometer and the results between experimental and numerical analyses were compared to produce a numerical model. Results comparisons showed good agreement where PEM demonstrated a 30% reduction in the resultant cutting force, improved surface roughness and 40% increased tool life compared with conventional turning. On the other hand, Wang et al. [3] combined plasma and cryogenic cooling of the workpiece within the conventional turning process of Inconel 718. They found that the surface roughness was reduced by 250%, the cutting forces were decreased by approximately 30%–50% and tool life increased by up to 170% over conventional cutting. However, PEM are widely used only in turning process. It is difficult to associate plasma heating in end-milling processes because the feed is relatively low and the workpiece will be melted due to the heat generated by the plasma arc.

6. Induction heating

Induction heaters provide alternating electric current to an electric coil (the induction coil). The induction coil becomes the electrical (heat) source that induces a high-frequency alternating electrical current into the workpiece to be heated. The heat is restricted to localized areas or surface zones immediately adjacent to the coil. This happens because the alternating current (a_c) in the induction coil has an invisible force field (or magnetic flux) around it. The induction coil actually functions as a primary transformer, with the workpiece to be heated becoming the secondary transformer. The force field surrounding the induction coil induces an equal and opposing alternating electric current in the workpiece [8]. The workpiece will be heated up due to the resistance to the flow of this induced high-frequency alternating electric current. The rate of workpiece heating is dependent on the frequency and intensity of the induced current, the specific heat of the material, the magnetic permeability of the material, and the resistance of the material to the flow of current. The induced currents are sometimes referred to as eddy currents, with the highest intensity current being produced within the area of the intense magnetic fields. The heating system consists of three major components high-frequency transformer (invertors), matching box (transformer and condenser) and cooling unit. The overall experimental setup is shown in Figure 7.

In contrast, Luo et al. [23] conducted experiments on conduction heating on end-milling cutting tools. The experiment is different compared to custom setups where the preheating temperature is applied on the cutting tool. This technique is more focused on machining nonconductive material such as elastomers, rubbers and plastics. Generally known nonconductive materials have lower melting points and it is impossible to apply preheating temperatures on those materials. Results from the experiment show that preheating the cutting tool will make the material softer and the machining accuracy becomes much better than conventional cutting. On the other hand, Kizaki et al. [24] proved that thermal-assisted machining is not applicable in the drilling process. As an alternatif technique, the tool was heated to reduce the vibration during drilling on zirconia material. The results showed that by preheating the cutting tool up to 500°C, the workpiece temperature could increase to 150°C–400°C. Finally, the cutting experiment demonstrated an improvement in machinability.

http://dx.doi.org/10.5772/61101

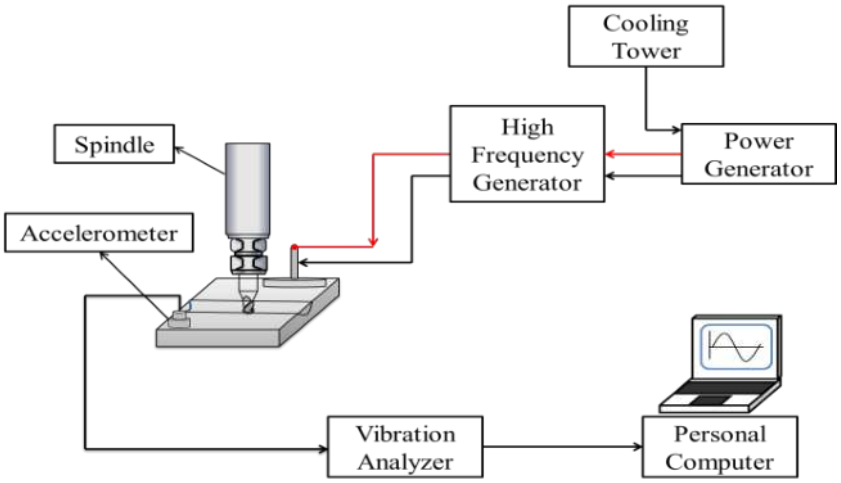

Figure 7. Overall experimental setup for induction heating machining.

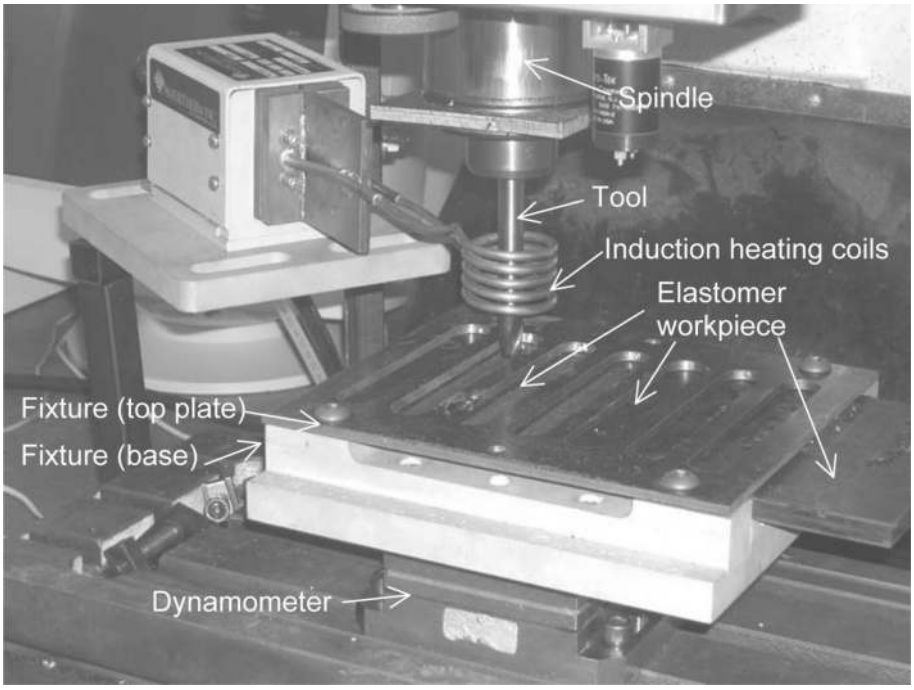

Figure 8. Experimental setup of elastomer end-milling with tool induction heating [23].

7. Laser-assisted milling

Laser-assisted milling is a hybrid machining process that combines preheating and mechanical removal processes. Many studies have been conducted using several types of lasers and milling machines. Most studies reported positive results with large improvements on tool life and lower cutting forces. However, in cases where material property preservation is crucially important, tool selection and heating temperature need to be perfectly mastered.

In the laser-assisted micromilling (LAMM) process, appropriate parameters need to be determined to ensure that the machining process can be performed at a higher level to produce microsize and highly accurate machined parts. The determination of machining parameters can be referred from the basic theory of LAMM as shown in Figure 9. The heating location generated by laser beam irradiation, T_{bc} and cutting tool, T_c must be well-determined to confirm that the heat generated is in the recommended temperature range for better softening effect (700°C). Mohid et al. [25] predicted the temperature distribution on pulsed laser mode by using ANSYS APDL software. From their results, it was concluded that by using a 140-W power laser, a beam-to-cutting tool distance of between 0.8 and 1.9 mm and a depth of 0.005 to 0.117 mm could be obtained. Yang et al. [26] have developed a 3D transient finite element method to predict the depth and width of HAZ on ductile material. It was found that the laser parameters, especially laser power, have strong influence on the depth and width of HAZ. In addition, Kim and Lee [27] used FEA to predict the preheating temperature on Inconel 718 and AISI 1045 materials to obtain the depth of cut.

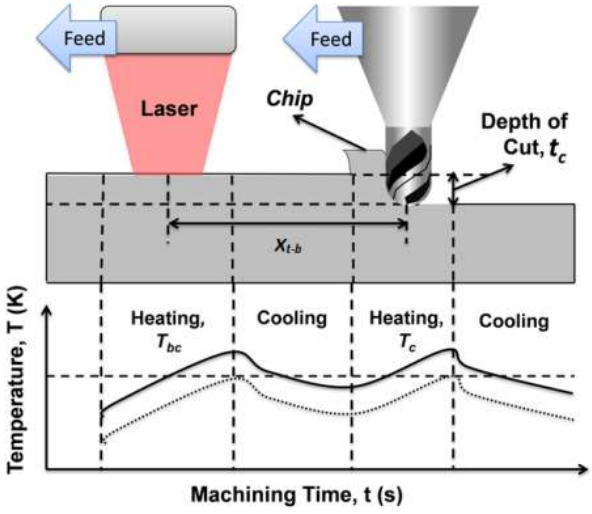

Figure 9. Theoretical analysis of LAMM.

Finite element analysis (FEA) was used to predict the temperature distribution on the top and bottom surfaces. The FEA model was developed by using ANSYS APDL software to predict

heat distribution during the laser irradiation process. At the same time, it creates the HAZ pattern underneath the workpiece surface. Based on workpiece temperature distribution, the range of laser spot-to-cutting tool distance $X_{t\text{-}b}$ and the depth of cut t_c can be determined prior to the actual machining process. It is essential to determine the initial tool engagement temperature as shown in Figure 10(a) and (b). It is intended to ensure that the preheating temperature will not impair the tool performance. This argument is supported by Kim and Lee [27], who reveal that by applying temperatures between 650°C and 900°C, the material strength will be significantly reduced. However, Rahim et al. [28] mentioned that the most prominent effect on cutting force, surface texture and tool wear, was defined by $X_{t\text{-}b}$. From their findings, they concluded that it is necessary to control the irradiation temperature. However, in this study, the $X_{t\text{-}b}$ was fixed at 600 μm in order to avoid the laser beam irradiation into the cutting tool. The workpiece temperature obtained from their study was approximately 400 K.

Higher average laser powers generated higher temperatures at the workpiece's surface. A melting region will be produced when the temperature generated reaches the melting point while a HAZ region forms when the temperature exceeds the deformation temperature. Rapid cooling at the upper surface will occur and make the material harder due to hardening effects. Meanwhile, the size of the thermally affected zone is small. The temperature gradient reaches high values at the upper surface and the heat distributed to the material underneath depends on the conduction rate value. However, the temperature value is expected to be considerably higher when the temperature is distributed into the solid bulk phase. This causes the temperature at the surface to decay rapidly once the laser beam passes over this region. This process is affected by the thermal conductivity of the substrate material [29].

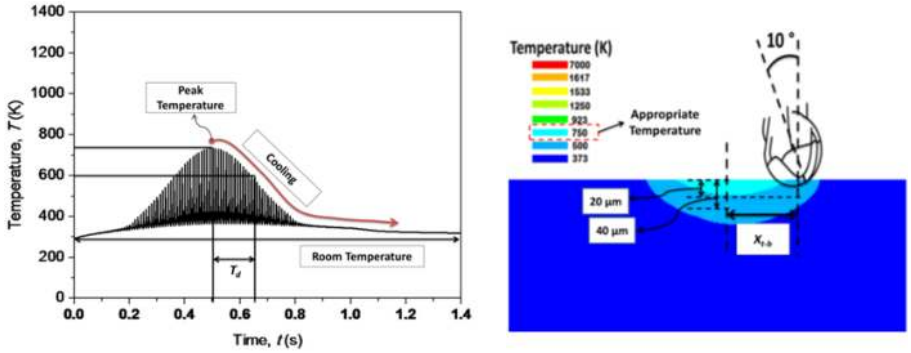

Figure 10. Results of temperature distribution when P_{avg} = 4.16 W, t_p = 1 ms and f_r = 70 mm/min, (a) recorded temperature at the centre irradiation line, (b) prediction of tool location and the depth of cut when using P_{avg} = 4.16 W, t_p = 1 ms, f_r = 70 mm/min, A = 32% [19].

The actual experimental setup of the LAM process is shown in Figure 11. An air-bearing spindle with a maximum rotation per minute of 60,000 is installed into the micromilling machine. All the laser-assisted micromilling tests were carried out on hardened Inconel 718

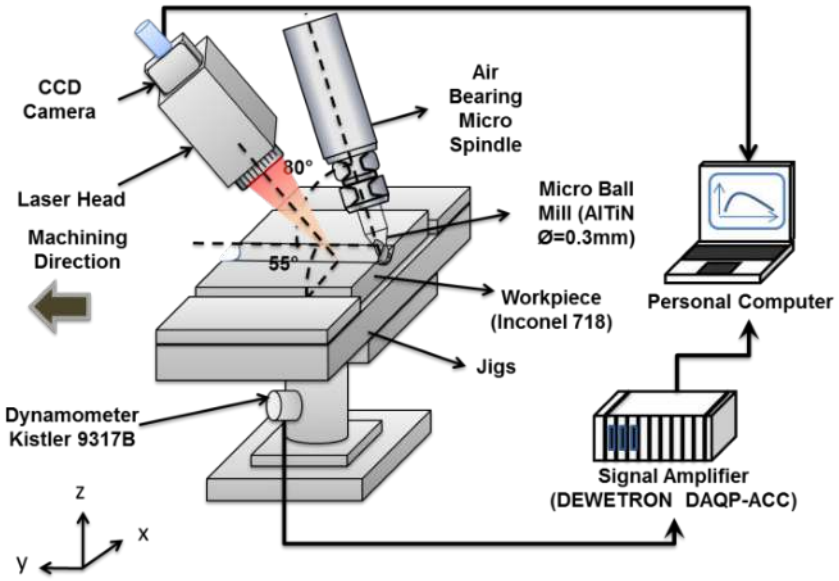

Figure 11. Experimental setup for laser-assisted milling [30].

plates (21–23 HRC) with 15 mm length, 40 mm width and 5 mm thickness. Commercially available AlTiN-coated carbide ball end mills (two flutes) with a diameter of 300 μm were used in cutting tests. The workpiece surface was preheated using Nd:YAG-pulsed laser with a 1064 nm wavelength. The laser head was inclined to 55° to avoid the deflection of laser irradiation on the cutting tool. The irradiated heat induced into the cutting tool will alter its properties. The dynamometer Kistler 9317B integrated with a DAQP-ADD card was used to measure the cutting force.

8. Laser-assisted turning

Laser-assisted turning process has attracted researchers for decades due to the demand for the machining of hard-to-cut materials. This technique was proven to reduce the cutting forces, obtain smoother machining surface and eliminate the production of continuous chips when the materials were produced under high cutting speeds.

Figure 12 shows the relative position of the laser beam, cutting tool and workpiece in the LAT process [31]. L_1 represent the distance between the focusing lens and the workpiece. The distance depends on the laser spot size being enough to cover the chamfer surface. While L_2 represent the distance between the tools' cutting edge and the laser spot point and it was determined by considering the heat effect on the tool. The actual initial cutting temperature is important to measure or predict. It will give a significant effect on cutting force results. In

actual turning cutting processes, the force component consists of feed force, radial force and cutting force. The actual reduction of cutting forces is dependent on the force component and cutting tool condition. Nevertheless, the force component was reduced by up to 30%. The determination of cutting force is required for [10] (i) estimation of cutting power consumption; (ii) machine development, fixture and tool system; (iii) evaluation of role of the various machining parameters (speed ($v_{c)}$, feed (f), depth of cut (DOC) and tool); (iv) understanding the behaviour and machinability characteristics of the work materials; (v) condition monitoring of the cutting tools and machine tools.

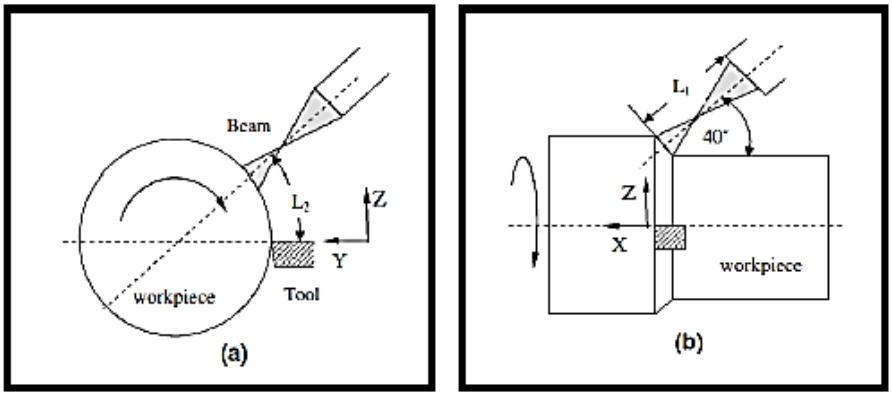

Figure 12. Relative position of laser beam, workpiece and cutting tool in LAT: (a) end view and (b) side view [32].

9. Influence of heat on nickel-based alloy

A huge demand on super alloys, especially Inconel 718, was significantly embarked by both heavy and microscale industries. Lasers and plasma are commonly used in thermally assisted machining of nickel-based alloys. It is a big challenge to determine the best method and optimum parameters to improve the machinability of super alloy materials in the machining process. Inconel has excellent material properties for high fatigue endurance limit, high yield strength, high corrosion resistance and high working temperature. The material can withstand machining temperatures of up to 700°C. This material is categorized as hard-to-machine because of the existence of carbide particles in its microstructure. Heating the material to higher than specific deformation temperatures will consequently harden the material with denser microstructure.

Since this material is weak in thermal conductivity, most of the heat generated in the cutting process will remain in the chip. The rest of the heat will be transferred into the base material and the cutting tool. This will lead to undesirable temperature increments during the machining process and further soften the material. However, in thermal-assisted machining, temper-

atures generated by friction between the tool and the workpiece are not favourable since it fluctuates with cutting speed and cutting depth changes. The accumulated heat energy could initiate microstructure changes onto the cutting surface. A well-controlled cutting temperature is needed to avoid the material from melting or being too soft, which promotes plastic deformation rather than ductile deformation during the cutting process. Applying cooling medium on the cutting tool during the plasma-assisted turning manages to reduce notching wear by 100%. The surface roughness can be improved by 150% to 250% for the tool life [3].

9.1. Cutting force

Figure 13 shows the effect of the depth of cut and laser-assisted micromilling (LAMM) of Inconel 718. In this experiment, the laser beam-to-cutting tool distance, $X_{t\text{-}b}$ was set at 600 μm. The results show that the thrust force significantly increases by increasing the t_c from 20 to 40 μm. When the t_c is increased from 20 to 40 μm, the centre part of the tool was rubbed on the workpiece surface and it consequently increased the cutting force. This is due to the absence of a cutting edge at the centre of the ball mill cutting tool. This phenomenon is prominent to produce rubbing and plunging processes. Otherwise, material properties also give significant effects due to the yield strength of the material, and it contributes to the increment of thrust force.

Irradiating Inconel 718 using an average laser power, P_{avg} of 4.16 W and $X_{t\text{-}b}$ of 600 μm, no melted region was observed but a HAZ effect is seen underneath the machined surface. Based on a review of the results shown in Figure 10(a) and (b), the peak temperature can be increased by up to approximately 800 K. This temperature is sufficient to reduce the material's strength. This argument is supported by Kim and Lee [13], and reveals that applying temperatures between 650°C and 900°C will reduce the material's strength significantly. Resulting from this irradiation, the thrust force was significantly reduced in all cases compared between LAMM and conventional cutting. However, in the case of LAMM using a micro ball mill tool at t_c of 40 μm, the thrust force drastically declined due to the increment of cutting tool effective-diameter and the changes in workpiece properties.

In addition, the changing trend of cutting force was also influenced by the spindle speed. The increment of spindle speed, N from 12,500 to 17,500 rpm, contributes to the higher cutting force. However, the trend shows contradiction when the spindle speeds decreased from 12,500 to 7500 rpm. Because higher spindle speeds produce higher contact ratios between the cutting edge and workpiece. However, at lower rpm, the cutting process is more effective in terms of material removal rate but with higher friction. Therefore, higher cutting temperatures were generated. This trend corresponds with the results presented by Arndt [33]. The author mentioned that the high cutting temperatures were due to the reactions of high shear resistance at high rpm. Meanwhile, the temperature still increases at low rpm, thus producing a strain-hardening effect.

Figures 13 and 14 show a comparison of cutting forces resulting between conventional machining and LAMM, respectively. It can be observed that the LAMM recorded the lowest value of force components at all tested conditions. Kong et al. [34] reported that laser-assisted machining successfully demonstrated the reduction of cutting force by around 30%–70% over

http://dx.doi.org/10.5772/61101

the conventional machining process. Because the heat generated by cutting and the lasers approached the melting point, and thus reduced the shear resistances. In addition, the laser beam's preheating process on the workpiece material is in the deformation temperature range and managed to initiate a softening effect [9].

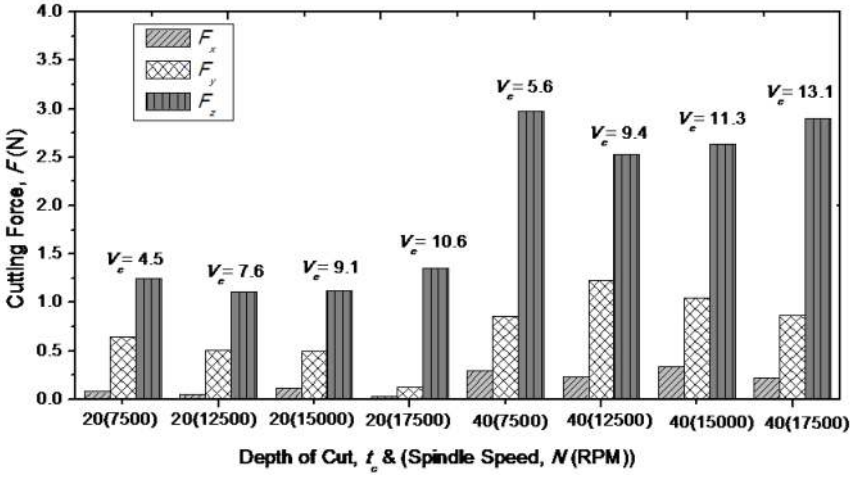

Figure 13. Results of cutting force at different cutting speeds, v_c, depth of cut, t_c and spindle speed, N in conventional micromilling process [30].

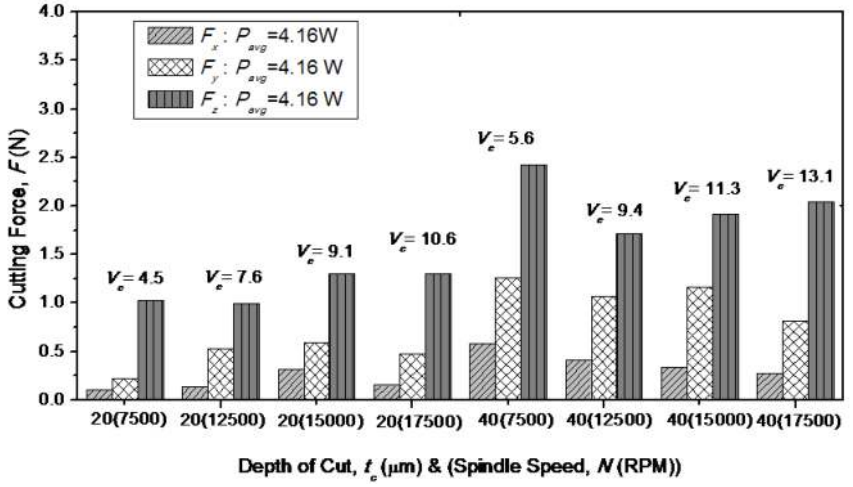

Figure 14. Results of cutting force at different cutting speeds, v_c, depth of cut, t_c and spindle speed, N in LAMM process [30].

9.2. Tool wear

Figure 15 shows a variation of wear patterns at all tested conditions. The image shows evidence that adhesion occurred on the flank face. Laser parameter and depth of cut give prominent effects on tool wear. The adhesion and coating delamination was critically increased when the depth of cut, t_c was increased from 20 to 40 μm under conventional machining processes. In addition, machining of ductile materials such as Inconel 718 using small ball mill diameters are inherently difficult processes. Once the adhesion is peeled off, it will cause a delamination of the coating and the tool loses its sharpness. This phenomenon is due to the material properties of Inconel 718 having a higher ductility and yield strength. According to Kuram and Ozcelik [35], most of the dominant wear mechanisms during micromilling of ductile materials were from abrasion and adhesion.

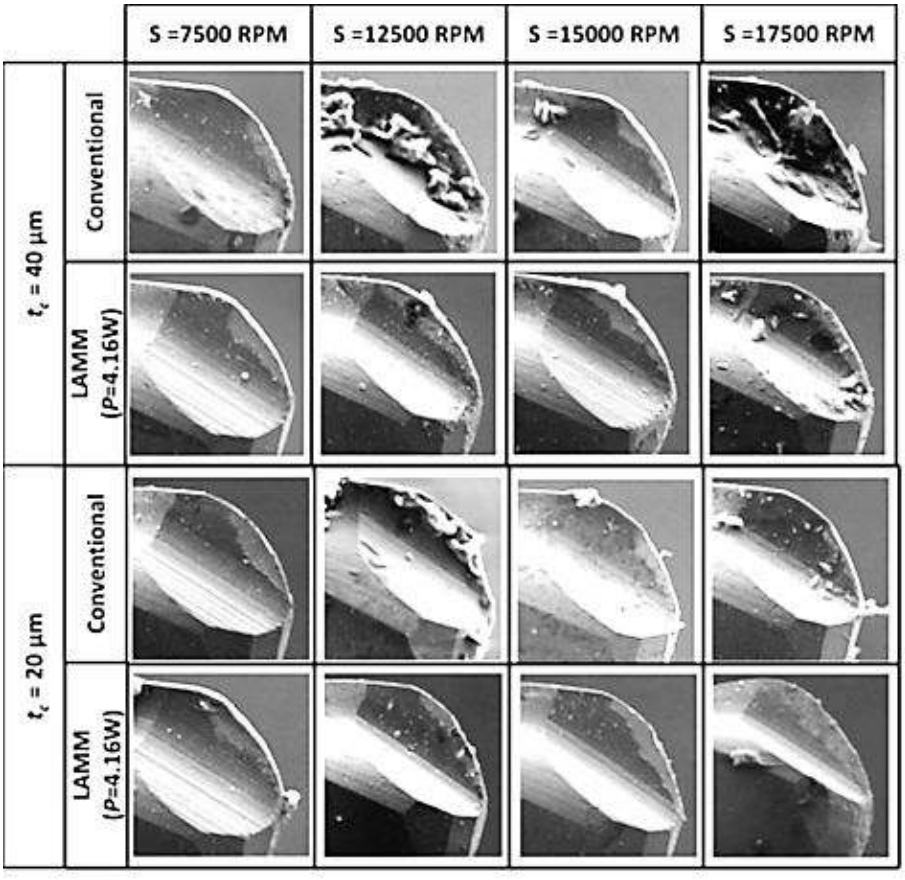

Figure 15. Tool wear on rack face of micro ball mill [30].

http://dx.doi.org/10.5772/61101

From these results, LAMM shows an improvement in terms of coating delamination and adhesion. The laser preheating method has shown its effectiveness in reducing the material strength and yield strength. During the irradiation process, surface material was preheated up to 900 K over the phase transformation of material. In this phase, the microstructure changes from γ' to γ'' as it dissolves the bonds between the particles [36]. These changes assist in avoiding material adherence at the tool rack face. Temporarily, adhered material on the cutting edge promotes the blunt cutting edge. However, in terms of ball end mill cutting tools, the effective of the cutting process at the bottom surface is poor and compels the rubbing process. Furthermore, the ineffectiveness of chip evacuation causes chips to re-enter the cutting region.

However, Kong et al. [34] investigated the effectiveness of coating material on laser-assisted milling of K24 nickel-based alloy. The amounts of average flank wear increases for both conventional machining and LAM with increasing cutting times are shown in Figure 16. However, the evolution of the flank wear is different between the two methods. The wear increases fast with the cutting time before 2.7 min, and is relatively stable from 2.7 to 16.8 min, after 16.8 min, rapid wear is visible again in LAM. The approximate machined times are 17.3 and 31.4 min for conventional machining and LAM tests, respectively, when the maximum wear criterion is set at VB_{ave} = 0.3 mm.

The results of laser-assisted milling experiments indicate that abrasive and adhesive wears were the most dominant wear mechanisms as shown in Figures 17 and 18. The TiAlN-coated tools exhibited the highest wear resistance at normal cutting speeds of 30 m/min. The triple-layer CVD-coated tool failure mode was concentrated on nonuniform flank wear due to the adhesion and depth-of-cut notching. TiCN performs poorly due to their inferior adhesion characteristics with the base material.

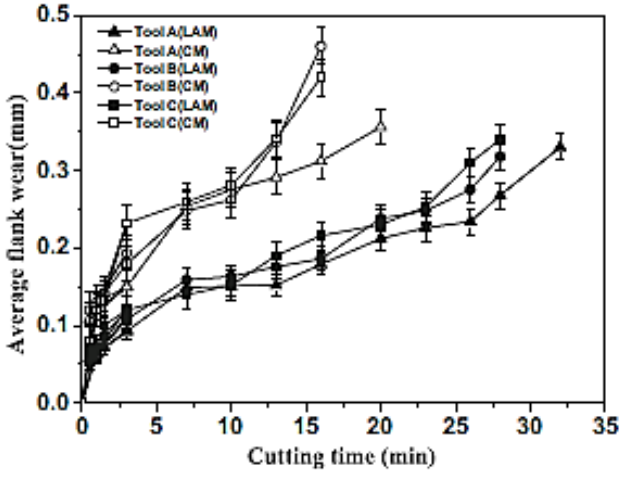

Figure 16. Results of the flank wear, in conventional machining and LAM, as a function of the cutting time [34].

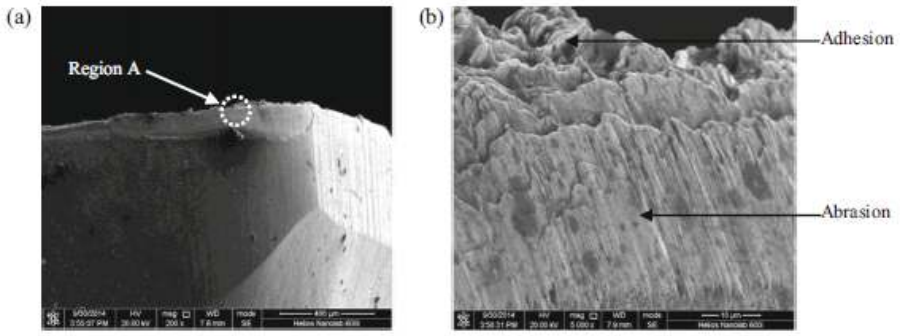

Figure 17. SEM of a TiAlN-coated tool at cutting speed V = 30 m/min and feed rate f = 0.10 mm/tooth with laser assist: (a) flank face at 10 s and (b) magnified SEM [34].

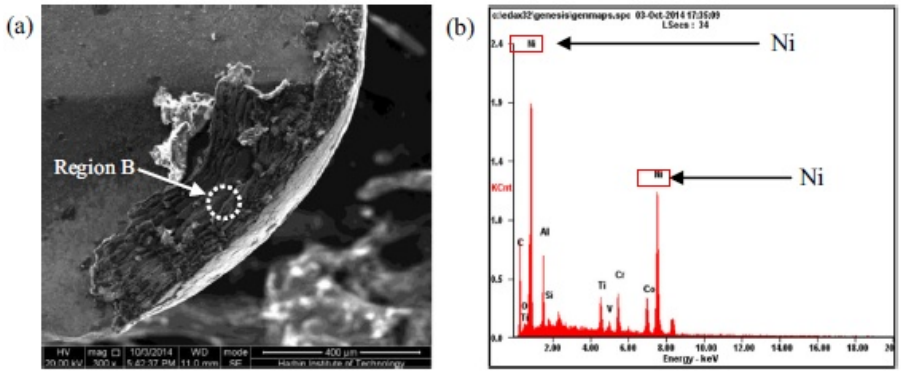

Figure 18. SEM of a TiAlN-coated tool at cutting speed V = 30 m/min and feed rate f = 0.10 mm/tooth with laser assist: (a) rack face at 10 s and (b) EDS of TiAlN-coated tool [34].

9.3. Surface roughness

Surface roughness in micromachining is recommended to be measured using noncontact measuring tools for accurate measurement. Figure 19 shows a comparison of the results of surface roughness between LAMM and conventional machining. The surface roughness values were measured using atomic force morphology (AFM) in three different points in order to obtain the roughness average, R_a.

It can be seen that the LAMM produces better surface roughness compared to the conventional machining process. In conventional machining processes, Inconel 718 retains its material properties with higher ductility and yield strength. Therefore, machinability is limited and the resulting rougher cutter mark at the bottom groove. Furthermore, conventional machining

http://dx.doi.org/10.5772/61101

also produced a burr on the upper side of the groove due to the build-up edge and ineffective chip removal. Higher ductility of material exacerbates the phenomenon.

In contrast, LAMM manages to produce a finer surface finish compared to conventional machining. The effective laser beam-to-cutting tool distance and lower power average creates an appropriate preheating temperature to reduce the yield strength. The variation of yield strength has consequently produced finer cutter marks at the bottom surface of the groove. According to Kiswanto et al. [37], feed rate and machining time gave significant effects on the surface roughness and burr formation. Longer machining times contributed to the tool wear or delamination. Consequently, poor surface finish was produced at the centre of the groove path.

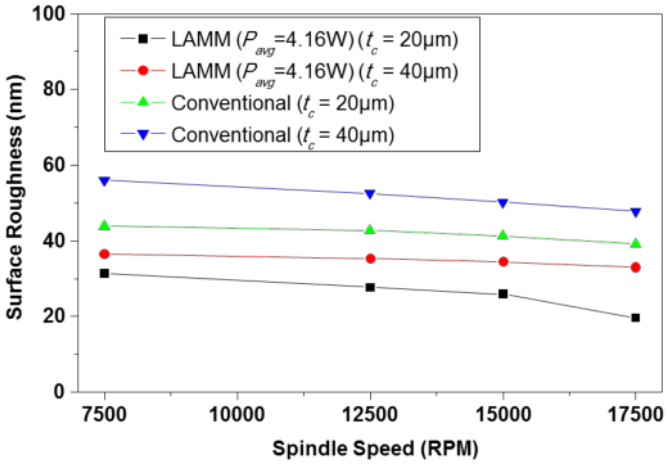

Figure 19. Comparison of surface roughness between LAMM and conventional machining processes [19].

10. Conclusion

The application of advanced materials in various parts fabrication has consequently increased the demand for new and high-performance machining techniques. Continuous study in material removal processing technique has shown that heating the workpiece is effective for increasing the machinability. The heat energy can be applied using several methods, either on the material or on the cutting tool, depending on the workpiece material behavior. The thermal-assisted machining technique is proven applicable on a wide range of material types including polymers and metals. The machinability of nickel-based alloys is proven to be improved by applying thermal machining technique. However, many studies were concentrated on turning process. A lot of issues can be explored and studied on milling process especially in microscale machining.

Author details

Erween Rahim*, Norazlan Warap and Zazuli Mohid

*Address all correspondence to: erween@uthm.edu.my

Advanced Machining Research Group, Universiti Tun Hussein Onn Malaysia, Parit Raja, Batu Pahat, Johor, Malaysia

References

[1] N. Waterman and M. Ashby, The Materials Selector, London: Chapman & Hall, 1997.

[2] M. Anderson, R. Patwa and Y. C. Shin. Laser-assisted machining of Inconel 718 with an economic analysis. *International Journal of Machine Tools & Manufacture,* vol. 46, pp. 1879–1891, 2006.

[3] Z. Y. Wang, K. P. Rajurkar, J. Fan, S. Lei, Y. C. Shin and G. Petrescu. Hybrid machining of Inconel 718. *International Journal of Machine Tools & Manufacture,* vol. 43, pp. 1391–1396, 2003.

[4] B. Shi, H. Attia, R. Vargas and S. Tavakoli. Numerical and experimental investigation of laser-assisted machining of Inconel 718. *Machining Science and Technology,* vol. 12, pp. 498–513, 2008.

[5] V. Ganta and D. Chakradhar. Multi objective optimization of hot machining of 15-5PH stainless steel using grey relation analysis. *Procedia Materials Science,* vol. 5, pp. 1810–1818, 2014.

[6] R. Muhammad, A. Maurotto, M. Demiral, A. Roy and V. V. Silberschmidt. Themelly enhanced ultrasonically assisted machining of Ti alloy. *CIRP Journal of Manufacturing Science and Technology,* vol. 7, pp. 159–167, 2014.

[7] G. Germain, P. D. Santo and J. L. Lebrun. Comprehension of chip formation in laser assisted machining. *International Journal of Machine Tools & Manufacture,* vol. 51, pp. 230–238, 2011.

[8] A. K. M. N. Amin, S. B. Dolah, M. B. Mahmud and M. Lajis. Effects of workpiece preheating on surface roughness, chatter and tool performance during end milling of hardened steel D2. *Journal of Materials Processing Technology,* vol. 201, pp. 466–470, 2008.

[9] H. Attia, S. Tavakoli, R. Vargas and V. Thomson. Laser-assisted high-speed finish turning of superalloy Inconel 718 under dry condition. *CIRP-Annal-Manufacturing Technology,* vol. 59, pp. 83–88, 2010.

[10] P. Y. Kok, A. K. M. N. Amin and A. I. Faris. Performance of preheating, cryogenic cooling and combined approachess in improving machinability of stainless steel in turning. In: *Proceedings of International Conference on Mechanical Engineering-ICME*, Dhaka, 2005.

[11] E. O. Ezugwu, Z. M. Wang and A. R. Machado. The machinability of nickel-based alloys: a review. *Journal of Materials Processing Technology,* vol. 86, pp. 1–16, 1999.

[12] M. Sundararaman, L. Kumar, G. E. Prasad, P. Mukhopadhyay and S. Banerjee. Precipitation of an intermetalic phase with Pt2Mo-type structure in alloy 625. *Metallurgical and Materials Transactions A,* vol. 30A, pp. 41–52, 1999.

[13] X. Luo., K. Shinozaki, S. Yoshihara, H. Kuroki and M. Shirai. Theoretical analysis of grain boundry liquation at HAZ of Inconel 718 alloy. *Quarterly Journal of the Japan Welding Society,* vol. 18-1, pp. 102–111, 2000.

[14] W. Konig and A. K. Zaboklicki. Laser-assisted hot machining of ceramics and composite materials. *International Conference on Machining of Advanced Materials,* vol. 847, pp. 455–463, 1993.

[15] S. Dharani and M. Pradip. Finite element analysis of laser irradiated metal heating and melting processes. *Optics & Laser Technology,* vol. 42, pp. 855–865, 2010.

[16] X. D. Ren, Q. B. Zhan, S. Q. Yuan, J. Z. Zhou, Y. Wang, N. F. Ren, G. F. Sun, L. M. Zheng, F. Z. Zhai, H. M. Yang and W. J. Dai. A finite element analysis of thermal relaxation of residual stress in laser shock processing Ni-based alloy GH4169. *Materials and Design,* vol. 54, pp. 708–711, 2014.

[17] Z. Mohid, N. M. Warap, M. I. S. Ismail, R. Ibrahim and E. A. Rahim. Determination of heat flux intensity distribution and laser absorption rate of AISI D2 tool steel. *Applied Mechanic and Materials,* vols. 465–466, pp. 730–734, 2014.

[18] Y. C. Shin and J. N. Kim. Plasma enhanced machining of Inconel 718. In: *Proceedings of the Manufacturing Science and Engineering, Symposium on Advanced Machining and Finishing Processes of Ceramics, Composites and High Temperature Alloys in ASME IMECE*, Atlanta, GA, 1996.

[19] E. A. Rahim, N. M. Warap, Z. Mohid, R. Ibrahim and N. Rafai. Numerical analysis of laser preheating for laser assisted micro milling of Inconel 718. *Applied Mechanics and Materials, vol 773-774, pp. 332-336, 2015*.

[20] A. J. Shih, M. A. Lewis and J. S. Strenkowski. End milling of elestomer-fixture design and tool effectiveness for material removal. *Journal of Manufacturing Science and Engineering,* vol. 126, no. 1, pp. 115–123, 2004.

[21] C. E. Leshock, J. N. Kim and Y. C. ShinPlasma enhanced machining of Inconel 718: modeling of workpiece temperature with plasma and experimental results. *International Journal of Machine Tools & Manufacture,* vol. 41, pp. 877–897, 2000.

[22] M. Madhavulu and B. Ahmed. Hot machining process for improved metal removal rates in turning operation. *Journal of Materials Processing Technology,* vol. 44, pp. 199–206, 1994.

[23] J. Luo, H. Ding and A. J. Shih, Induction-heated Tool Machining of Elastomers-Part 2: Chip Morphology, Cutting Forces and Machined Surface, *Machining Science and Technology: An International Journal,* vol. 9, pp. 567-588, 2005.

[24] T. Kizaki, K. Harada and M. Mitsuishi. Efficient and precise cutting of zirconia ceramics using heated cutting tool. *CIRP Annals - Manufacturing Technology,* vol. 63, pp. 105–108, 2014.

[25] Z. Mohid, N. M. Warap, S. Hassan, M. I. S. Ismail, R. Ibrahim and E. A. Rahim, Numerical Analysis of Laser Heating for Laser Assisted Micro Milling Application, *Applied Mechanics and Materials,* Vols. 465-466, pp. 720-724, 2014.

[26] J. Yang, S. Sun, B. Milan and W. Yan, Experimental investigation and 3D finite element prediction of the heat affected zone during laser assisted machining of Ti6Al4V alloy, *Journal of Materials Processing Technology,* vol. 210, pp. 2215-2222, 2010.

[27] D. H. Kim and C. M. Lee, A study of cutting force and preheating-temperature prediction for laser-assisted milling of Inconel 718 and AISI 1045 steel, *International Journal of Heat and Mass Transfer,* vol. 71, pp. 254-274, 2014.

[28] E. A. Rahim, Z. Mohid, N. M. Warap, M. R. Ibrahim and a. M. I. S. Ibrahim, A Prediction of Laser Sport-to-Cutting Tool Distance in Laser Assisted Micro Milling, in *International Conference of Micro Manufacturing*, Singapore, 2014.

[29] M. W. Norazlan, Z. Mohid and E. A. Rahim. Laser assisted machining of titanium alloys. *Materials Science Forum,* vol. 763, pp. 91–106, 2013.

[30] E. A. Rahim, N. M. Warap, M. Z. and R. Ibrahim. Investigation on laser assisted micro ball milling of Inconel 718. *Applied Machanics and Materials,* vol. 660, pp. 79–83, 2014.

[31] S. Sun, M. Brandt and M. S. Dargusch. The effect of laser beam on chip formation during machining of Ti6Al4V alloy. *The Minerals, Metals & Society and ASM International,* vol. 41, p. 1681, 2010.

[32] S. Sun, J. Harris and M. Brandt. Parametric investigation of laser-assisted machining of commercially pure titanium. *Advanced Engineering Materials,* vol. 10, pp. 565–572, 2008.

[33] G. Arndt. Ultra-high-speed machining: a review and analysis of cutting forces. *Proceedings of the Institution of Mechanical Engineers,* vol. 187, pp. 625–634, 1973.

[34] X. Kong, L. Yang, H. Zhang, K. Zhou and Y. Wang. Cutting performance and coated tool wear mechanisms in laser-assisted milling K24 nickel-based superalloy. *International Journal Advanced Manufacturing Technology,* vol. 9, p. 6606, 2014.

[35] E. Kuram and B. Ozcelik. Multi-objective optimization using Taguchi based grey relational analysis for micro milling of Al 7075 material with ball nose end mill. *Measurement*, vol. 46, pp. 1849–1864, 2013.

[36] W. Hongjie, I. Kenji, T. Makoto and I. Akio. Microstructure of Inconel 718 alloy subjected to rapid thermal and stress cycle - Joint performance controlling factor in friction welding of Inconel 718 alloy. *Welding International*, vol. 26, no. 2, pp. 152–158, 2009.

[37] G. Kiswantoa, D. L. Zariatina and T. Ko., "The effect of spindle speed, feed-rate and machining time to the surface roughness and burr formation of aluminum alloy 1100 in micro-milling operation," *Jou nal of Manufacturing Processes*, vol. 16, no. 4, pp. 435-450, 2014.